Zeolite structure descriptor for guiding the synthesis of efficient titanosilicalites through matching Ti sites and framework topologies for 1-Hexene epoxidation

Xuliang Deng [a], Dong Lin [b,*], Yang Xu [a], Xiang Feng [a,*], De Chen [a,c], Chaohe Yang [a,*], Honghong Shan [a]

[a] *State Key Laboratory of Heavy Oil Processing, China University of Petroleum, Qingdao 266580, China*
[b] *Max Planck-Cardiff Centre On the Fundamentals of Heterogeneous Catalysis FUNCAT, Cardiff Catalysis Institute, School of Chemistry, Cardiff University, Cardiff CF103AT, United Kingdom*
[c] *Department of Chemical Engineering, Norwegian University of Science and Technology, Trondheim 7491, Norway*

A R T I C L E I N F O

Keywords:
Metal-containing zeolite
Structure descriptor
Local framework disturbance index
Olefin epoxidation
Titanosilicalite

A B S T R A C T

Rational design of metal-containing zeolites with different framework topologies can boost catalytic performance, but the successful synthesis of metal-containing zeolites typically requires selection of suitable zeolite scaffolds. Herein, a zeolite structure descriptor (i.e., the local framework disturbance index, LFDI) is proposed to guide the design of Ti-containing zeolites by matching Ti sites and different framework topologies to enhance olefin epoxidation performance. Theoretical calculations of the incorporation of Ti metal atoms into different crystallographic T sites indicate that the BEA framework exhibits the more negative average substitution energy (-0.50 eV) than MFI and MEL frameworks due to the lowest average LFDI (3.14). As expected, the BEA framework showed the highest capacity of framework Ti species than MFI and MEL frameworks by atom-planting method. This high framework Ti content demonstrated outstanding 1-hexene epoxidation performances (TON: 1827.5). This work paves the way to rationally design Ti-containing zeolites by atom-planting method for epoxidation reactions.

1. Introduction

Zeolites are considered as the ideal scaffolds for the metal incorporation into the different framework topologies due to its ordered porous channel, spatial confinement effect and hydrothermal stability [1–6]. The synthesized metal-containing zeolites with unique single sites in the framework exhibit outstanding reaction performances [7–9], including unique shape selectivity, enhanced reaction activity, superior hydrothermal and thermal stability together with excellent recyclability. As a result, they have tremendous potential in a wide range of fields, including catalysis, gas storage, separation, and sensing [10–15]. To date, the International Zeolite Association (IZA) has certified 255 different framework topologies. Significant efforts have been devoted to selecting, tailoring, and realizing the match between different metal sites (i.e., framework and extra-framework species) and zeolite scaffolds across these 255 topologies [16–27].

The atom-planting strategy which is considered as one of the most important synthetic method for metal-containing zeolites is emerging due to the high metal loading, highly-efficient and short synthetic period, and incorporated metal atoms with large radius (e.g., Ti, Sn and Zr) [1]. One of the most important active sites among these topologies is the metal Ti atom confined within the zeolite framework, which is known as titanosilicalite [28–30]. Titanosilicalite could be widely applied to the cyclohexanone ammoxidation, selective oxidation of alkanes, phenol hydroxylation, oxidation of alcohol and olefin epoxidation due to the unique oxidation ability of framework Ti atoms [31–35]. Among them, olefin epoxidation is a critical reaction in chemistry due to its ability to produce epoxides containing active three-member epoxy rings. 1,2-epoxyhane is a crucial oxygen-containing derivative produced from the epoxidation of 1-hexene, serving as a raw material for numerous high-value chemical products such as polyester fibers, pharmaceutical intermediates and cosmetic additives [36,37]. Moreover, the 1,2-hexanediol produced by the hydrolysis of 1,2-epoxyhexane can also have a wide application in the synthesis of printing ink, pharmaceutical

* Corresponding authors.
E-mail addresses: LinD6@cardiff.ac.uk (D. Lin), xiangfeng@upc.edu.cn (X. Feng), yangch@upc.edu.cn (C. Yang).

intermediate, oil paint, and detergent [38,39]. Therefore, the epoxidation of 1-hexene to synthesize 1,2-epoxyhane is gradually gaining importance in industry due to its significant industrial applications. Designing efficient Ti-containing catalysts for 1-hexene epoxidation is of prime scientific and industrial significance.

Despite the availability of different framework topologies (e.g., MFI, MEL, and BEA) for incorporating Ti atoms [40–43], screening of the most suitable structure for Ti incorporation by atom-planting method requires numerous experiments due to the easy formation of extra-framework TiO_2 species. Additionally, there is still a lack of quantitative judgment of the Ti incorporation at the atomic scale of framework topologies. Therefore, the zeolite structure descriptor to guide the design of efficient Ti-containing zeolites is indispensable and highly desired.

In this work, the rational design strategy of titanosilicalites with different framework topologies based on the zeolite structure descriptor is first proposed by theoretical calculation. The local framework disturbance index (LFDI) is used to describe the matching degree between the metal Ti atoms and different framework topologies. The LFDI is positively related to the substitution energy and reaction energy during the incorporation of Ti atoms. It is found that the BEA framework with the lowest average LFDI of 3.14 and lowest average substitution energy of −0.50 eV shows the highest capacity of framework Ti species. The relative content of framework Ti species in BEA synthesized by atom-planting method is 97.3 %. The Ti-β with rich framework Ti species shows outstanding 1-hexene epoxidation performances with a TON of 1827.5 and selectivity of 95.4 %. This rational design strategy could be used to guide the synthesis of high-efficient metal-containing zeolite by atom-planting method without requiring excessive experiments.

2. Experimental section

2.1. Synthesis of titanosilicalites by atom-planting method

The synthesis of titanosilicalites was based on the dealumination process and further Ti atom-planting method. The atom-planting strategy is the suitable method to compare the ability for Ti incorporation. It is widely known that without the inclusion of supplementary additives (e.g., F^- or OH^- anions as mineralizers), Ti-β cannot be synthesized via the conventional hydrothermal synthesis method [44–46]. To ensure equitable comparisons, the identical atom-planting strategy was consistently applied in the preparation of all titanosilicalites, namely TS-1, TS-2, and Ti-β without any additives [47–49]. In the process of dealumination, 1 g of zeolites (ZSM-5, ZSM-11 and β zeolites) were added into the 25 mL HNO_3 solution (13 mol/L) under strong magnetic stirring. The ZSM-5, ZSM-11 and β zeolites with similar Si/Al ratios of ~ 15 (Table S3) were all bought from the Catalyst Factory of Nankai university. Then this solution was heated at 100 °C for 24 h. After that, the suspension liquid was centrifuged and dried at 90 °C overnight. The white powder was further calcinated at 550 °C for 3 h to obtain dealuminized zeolites. Subsequently, these dealuminized zeolites were mixed with 10 mL of ethanol solution containing specific content of $TiCl_4$. The above-mentioned mixed solution was stirred for 6 h and then dried at 90 °C overnight. Finally, the as-synthesized titanosilicalites were calcinated at 550 °C for 3 h. For example, the obtained white powder was denoted as 0.1 %Ti-β which represents the β zeolites containing 0.1 wt% Ti content.

2.2. Catalytic test in the 1-hexene epoxidation

In the catalytic test of 1-hexene epoxidation, firstly, 0.2 g of catalyst was added into the 20 mL of acetonitrile gradually. Subsequently, 1.2 g of 1-hexene and 1.2 g of 30 wt% H_2O_2 were added into the above-mentioned mixture. Then, the reaction of 1-hexene epoxidation was tested at 60 °C for 180 min under strong magnetic stirring.

The related reactants and products were all detected by the gas chromatography (Agilent 6890) equipped with the HP-5 column and an FID detector. The moles of reactants and products were obtained by standard curves with the internal standard (m-xylene). It is essential to recognize that the introduction of TON was necessitated by the similarity in conversion rates. A higher TON indicates improved reaction efficiency for each titanium site under conditions of comparable conversion rates. Consequently, TON serves as a robust metric for comparing the average activity of each titanium site. The calculation of TON and selectivity were according to the following formulas:

(1) 1,2-epoxyhexane selectivity:
$$= \frac{moles\ of\ 1,2-epoxyhexane}{moles\ of\ 1-hexene\ before\ the\ reaction - moles\ of\ 1-hexene\ after\ the\ reaction} \times 100 \quad (1\text{–}1)$$

(2) (2) TON: =
$$\frac{moles\ of\ 1,2-epoxyhexane}{moles\ of\ Ti\ atoms} \quad (1\text{–}2)$$

(3) (3) Conversion of 1-hexene:
$$= \frac{moles\ of\ 1-hexene\ after\ the\ reaction}{moles\ of\ 1-hexene\ before\ the\ reaction} \times 100 \quad (1\text{–}3)$$

(4) (4) Conversion of H_2O_2:
$$= \frac{moles\ of\ H2O2\ after\ the\ reaction}{moles\ of\ H2O2\ before\ the\ reaction} \times 100 \quad (1\text{–}4)$$

(5) (5) H_2O_2 utilization efficiency:
$$= \frac{conversion\ of\ 1-hexene}{conversion\ of\ H2O2} \times 100 \quad (1\text{–}5)$$

2.3. Characterizations

The crystal structures of zeolites with different framework topologies were characterized by the X-ray diffraction (XRD, PANalytical Company, Netherlands) with a Cu K_α radiation. The X-ray diffraction was equipped with a 2D plane detector (PIXcel3D universal matrix detector). The scanning speed is about 10°/min. The diffuse reflectance spectra of the composites, which reveal the presence and relative quantities of Ti species, were obtained using the ultraviolet–visible (UV–Vis) spectrophotometer from SHIMAZU, Japan. As a reference, $BaSO_4$ was utilized. To capture the signals, the TS-1 sample was pressed against a $BaSO_4$ background and employed in conjunction with an integrating sphere accessory to enhance signal reflection. The relative percentage of framework Ti species in all Ti species is calculated based on the Gaussian fitting method (three Gaussian profiles: tetrahedral Ti at 220 nm, hexagonal Ti at 260 nm and anatase TiO_2 species at 320 nm). The framework Ti species located at 980 cm^{-1} of different zeolites was determined by the Fourier transform infrared spectroscopy (FT-IR, Nicolet, IS30) and the KBr was used as the blank sample. FT-IR spectra were acquired by employing the conventional transmission technique with KBr pellets. The morphology and elementary distribution of titanosilicalite particles were both revealed by the transmission electron microscope (TEM, JEOL, JEM-2100UHR). Approximately 30 mg of samples was placed into a polypropylene sample holder with a 1 cm diameter, which was then sealed using ultralene film. These prepared samples were subsequently inserted into a spectrometer (Shimadzu, EDX-7000) with a sample chamber that had been purged with high-purity helium (He), before the measurements were conducted.

2.4. Density functional calculation

The Vienna Ab-initio Simulation Package (VASP, Materials Design company, Austria) was used for the density functional calculation (DFT). The exchange–correlation energy function is the GGA-PBE with a cut-off energy of 400 eV. The projected augmented wave potentials were further used to describe the interaction between the core and valence electron. According to the MFI structure, a 95 T ($Si_{95}O_{150}H_{84}$) model was constructed for the pure siliceous zeolite. The cell parameters of the 95 T cluster model are as follows: α = β = λ = 90°, a = b = c = 25 Å. According to the MEL structure, a 79 T ($Si_{79}O_{123}H_{74}$) model was constructed for the pure siliceous zeolite. According to the BEA structure, a 42 T ($Si_{42}O_{63}H_{50}$) model was constructed for the pure siliceous zeolite. The H atoms were used to coordinate with the terminal Si atoms. The Ti atoms were incorporated into the different sites to construct

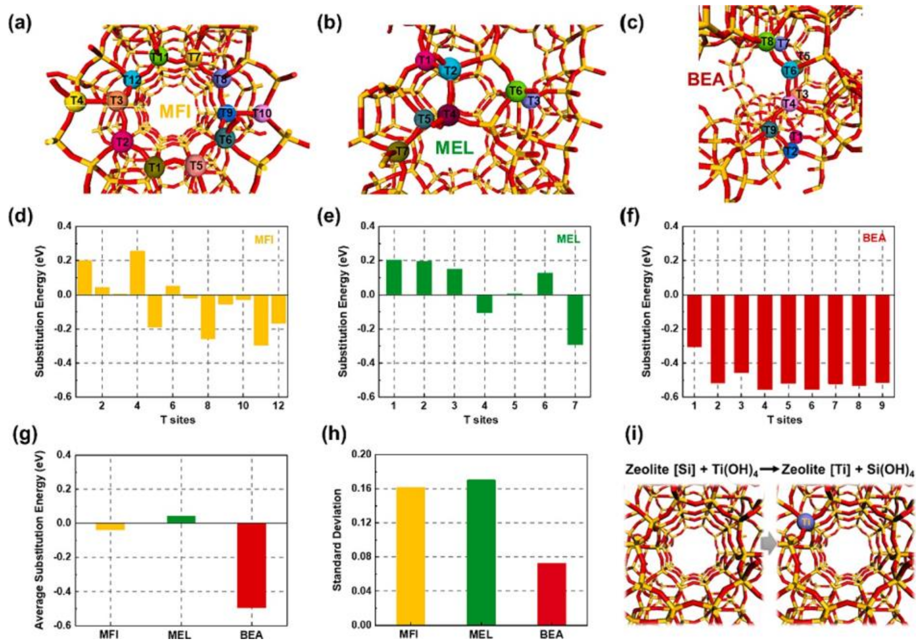

Fig. 1. The schematic diagram of different T sites in the (a) MFI framework topology, (b) MEL framework topology and (c) BEA framework topology. The substitution energy at different T sites by Ti atom in the (d) MFI framework topology, (e) MEL framework topology and (f) BEA framework topology. (g) The average substitution energy by Ti atoms in the MFI, MEL and BEA framework topologies. (h) The standard deviation of substitution energy by Ti atoms in the MFI, MEL and BEA framework topologies. (i) The schematic diagram of substitution by Ti atom in the zeolite framework.

titanosilicalites. Due to the large model of different zeolites, the K point was set to be 1 × 1 × 1 at the Γ point. The DFT-D3 correction method was used to calculate the dispersive interactions. The plane-wave basis was used for the expansion of Kohn-Sham orbitals. Moreover, the structure and energy optimization will be stopped until the force was lower than 0.03 eV/Å and the energy was lower than 1×10^{-5} eV in adjacent steps, respectively.

3. Results and discussion

3.1. Zeolite structure descriptor for the incorporation of Ti atoms

In order to study the incorporation of Ti atoms into the zeolite framework, the typical MFI, MEL and BEA framework topologies were used to reveal the effect of zeolite structure for the incorporation of Ti atoms based on the DFT calculation. For the different zeolite structures, the MFI, MEL and BEA framework topologies have 12, 7 and 9 different T sites [50,51], respectively (Fig. 1a–c).

The substitution process shown in Fig. 1i was used to represent the incorporation of Ti atoms into the different zeolite frameworks. The substitution energy could be used to determine the preferred location and framework of Ti atoms in different topologies. The substitution energy could be calculated according to the following equation [52]:

$$E_{SE} = E_{zeo[Ti]} + E_{Si(OH)_4} - E_{zeo[Si]} + E_{Ti(OH)_4} \quad (1)$$

In the equation (1), the $E_{Si(OH)_4}$ and $E_{Ti(OH)_4}$ represent the electronic energies of $Si(OH)_4$ and $Ti(OH)_4$, respectively. The $E_{zeo[Ti]}$ and $E_{zeo[Si]}$ are the electronic energies of titanosilicalite and silicalite, respectively.

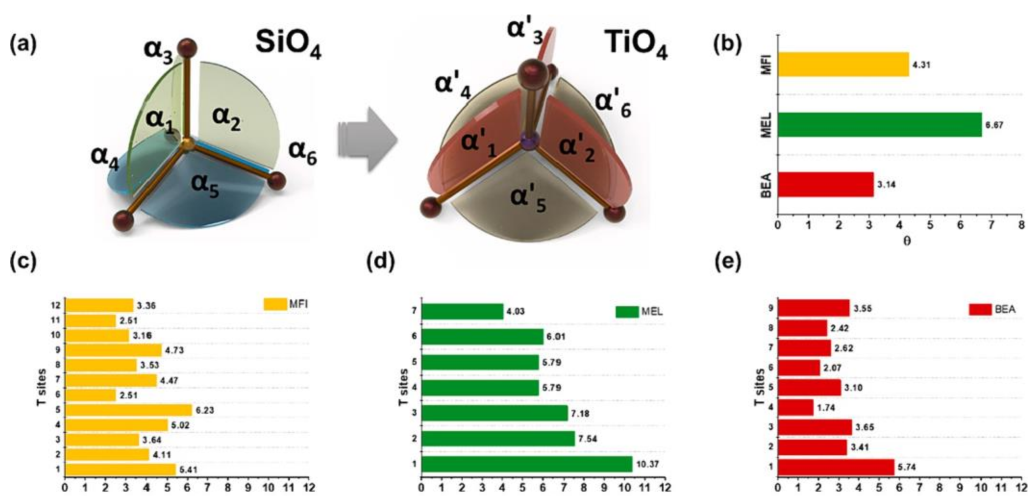

Fig. 2. (a) The schematic diagram of six angles in SiO_4 and TiO_4 groups in the zeolite framework. (b) The average local framework disturbance index (LFDI) in different framework topologies. The LFDI in different T sites of (c) MFI, (d) MEL and (e) BEA framework topologies.

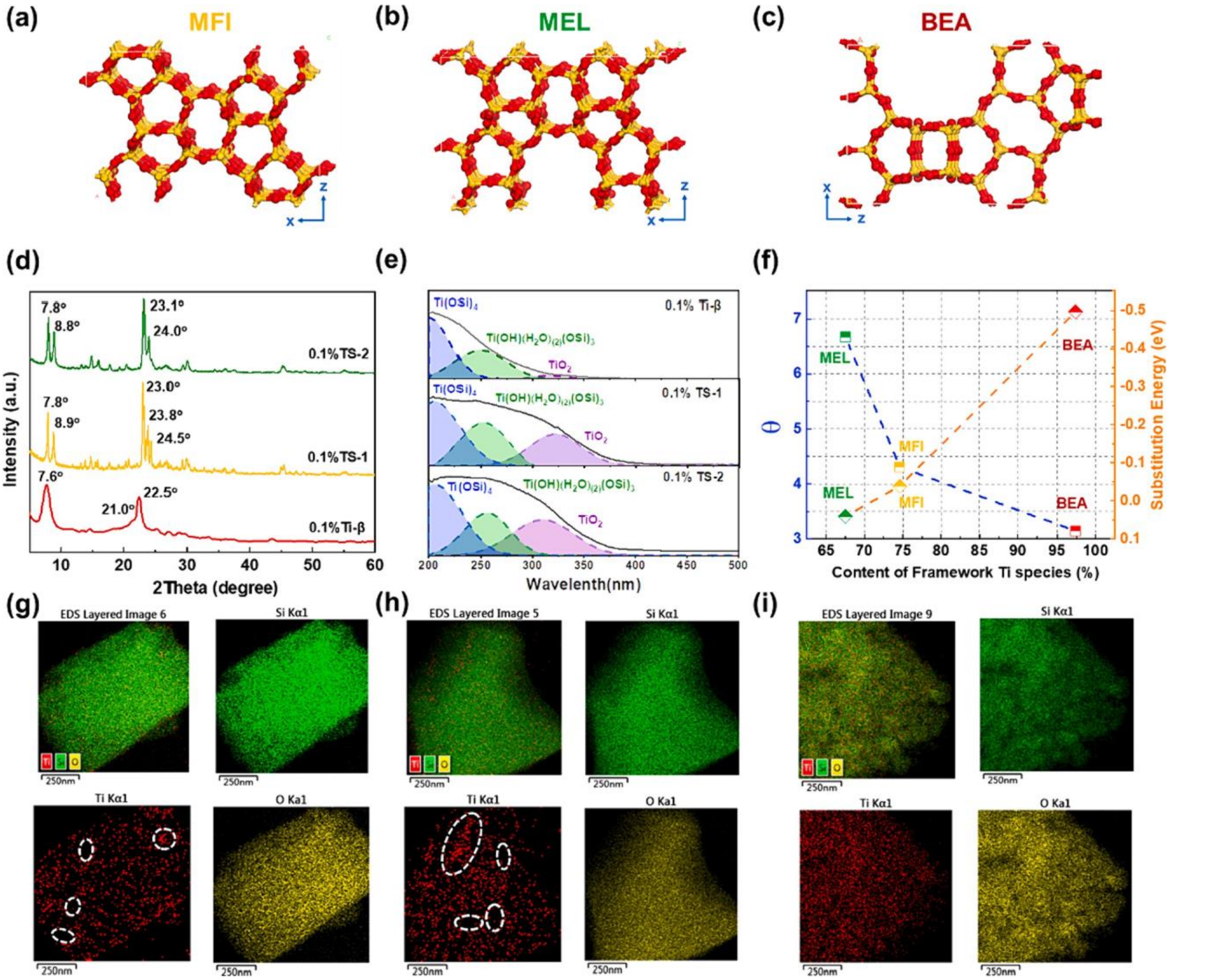

Fig. 3. The structural diagram of (a) MFI, (b) MEL and (c) BEA framework topologies. The (d) XRD patterns and (e) UV–vis spectra of Ti-β with BEA framework, TS-1 with MFI framework and TS-2 with MEL framework. (f) The relationship between the content of framework Ti species, substitution energy and LFDI (θ). The TEM-Mapping of (g) TS-1 with MFI framework (h) TS-2 with MEL framework, (i) and Ti-β with BEA framework.

Thus, the E_{SE} represents the substitution energy and the lower value indicated that the corresponding Ti-incorporated framework is more stable.

For 12 different T sites in the MFI framework topology (Fig. S1a–l), there are 5 T sites (T1, T2, T3, T4 and T6) that have positive substitution energies and 7 T sites (T5, T7, T8, T9, T10, T11 and T12) that have negative substitution energies (Fig. 1d). The substitution energies of T5, T8, T11 and T12 sites are −0.19, −0.26, −0.30 and −0.17 eV, respectively. These four sites are preferred locations with significantly lower substitution energies than other sites (T7: −0.02 eV, T9: −0.05 eV, T10: −0.03 eV) in the MFI framework topology. Moreover, the substitution energies of 7 different T sites in the MEL framework topology were also calculated (Fig. S2a–g). The T4 and T7 sites are preferred locations with negative substitution energies (-0.10 and −0.29 eV) shown in Fig. 1e. There are also 5 different T sites (T1, T2, T3, T5 and T6) with positive substitution energies. Differently, the substitution energies of 9 different T sites in the BEA framework topology (Fig. S3a–i) were all negative and lower than −0.30 eV in Fig. 1f. The energy required for substitution at the T1 site is comparatively greater than that at other sites, making other sites more preferable for incorporation into the framework.

The average substitution energy was further calculated in Fig. 1g to compare the compatibility between the metal Ti atom and different framework topologies. The BEA framework topology has the best compatibility with the lowest average substitution energy of −0.50 eV. The average substitution energy follows the following order: MEL (0.04 eV) > MFI (-0.04 eV) > BEA (-0.50 eV). The standard deviation of substitution energy was further used to show the dispersion of substitution energy in different T sties (Fig. 1h). It is found that the BEA framework topology has the lowest standard deviation (0.0725) than MFI and MEL framework topologies. The lowest standard deviation demonstrated that substitution energies in different T sites were closer to the lowest average substitution energy of −0.50 eV than other framework topologies. Therefore, BEA framework topology not only has the lowest average substitution energy but also the narrowest distribution of substitution energy, thus providing more preferred locations than MFI and MEL framework topologies.

In order to further reveal the intrinsic reason of different substitution energies in different framework topologies, the local framework disturbance index (LFDI) was introduced. Compared with the change of bond length between SiO_4 and TiO_4 groups, the change of six angles between SiO_4 and TiO_4 groups could have greater impact on the structural perturbation of zeolite framework during Ti substitution process. The LFDI (θ) could be calculated based on the six angles before and after Ti incorporation (Fig. 2a) according to the following equation:

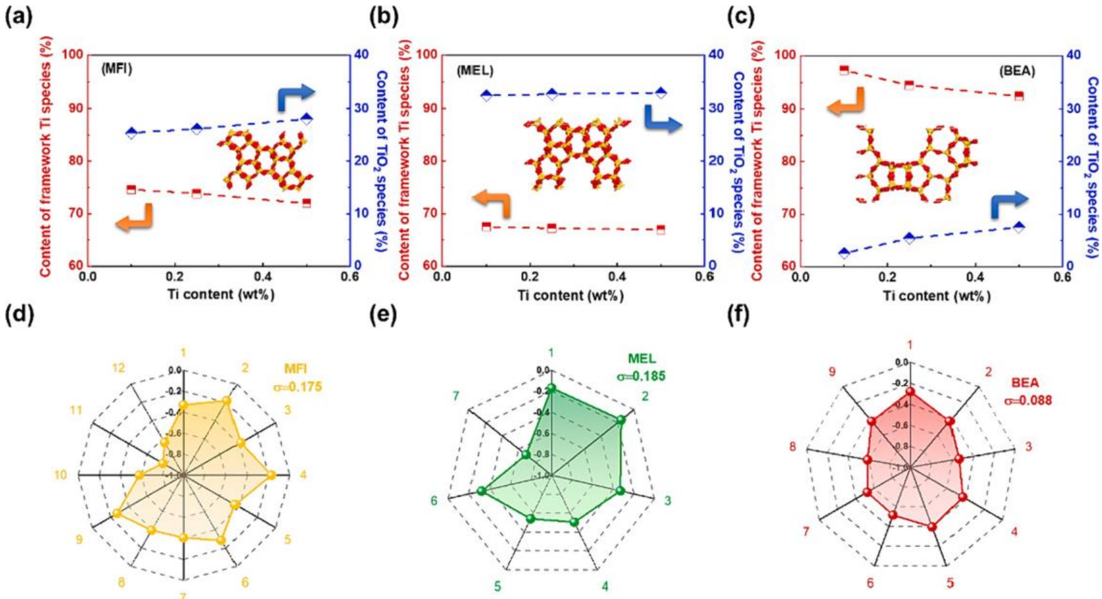

Fig. 4. The relationship between the Ti content, framework Ti species and TiO_2 species in the (a) MFI, (b) MEL and (c) BEA framework topologies. The reaction energy in different T sites of the (d) MFI, (e) MEL and (f) BEA framework topologies.

$$\vartheta = \sqrt{\sum_{i=1}^{i} (\alpha_i - \alpha)^2} \qquad (2)$$

The LFDI could be used to quantitively determine the structural perturbation aroused by the Ti incorporation into the zeolite framework. The LFDI of different T sites in the MFI, MEL and BEA framework topologies were shown in Fig. 2c–e. It is found that the BEA framework topology has the lower LFDI in terms of overall trends. The average LFDI was further calculated to quantitively compare the degree of structural perturbation in different zeolite frameworks. The average LFDI represented by θ shown in Fig. 2b follows the following order: MEL (6.67) > MFI (4.31) > BEA (3.14). This sequence of average LFDI is in accordance with the average substitution energy. The weaker structural perturbation could effectively stabilize the zeolite framework after Ti incorporation, thus decreasing the substitution energies. Therefore, the BEA framework topology with lower average LFDI and average substitution energy is the more ideal scaffold for the Ti incorporation than MFI and MEL framework topologies. The substitution energy is primarily determined by the Ti incorporation process, reflecting a surface-level phenomenon. To attain more comprehensive understandings in substitution energies, it is imperative to undertake further investigations. Consequently, we advocate the utilization of the Local Framework Disturbance Index (LFDI) to elucidate the structural perturbations within the zeolite framework during the Ti substitution process, as this constitutes the fundamental factor driving alterations in substitution energies.

3.2. Synthesis of titanosilicalites with different framework topologies

The titanosilicalites with MFI, MEL and BEA framework topologies (Fig. 3a–c) were further synthesized by atom-planting method to demonstrate the rational design of Ti-containing zeolites based on the zeolite structure descriptor (LFDI). The atom-planting strategy is the suitable method to compare the ability for Ti incorporation, which is because Ti-β cannot be synthesized via the conventional hydrothermal synthesis method without the inclusion of supplementary additives (e.g., F^- or OH^- anions as mineralizers). These additives could boost the nucleation, crystallization and further growth [53,54]. To ensure equitable comparisons, the identical atom-planting strategy was consistently applied in the preparation of all titanosilicalites, namely TS-1, TS-2, and Ti-β without any additives.

In Fig. 3d, the 0.1 %TS-1 catalyst shows five typical diffraction peaks at 2θ = 7.8°, 8.9°, 23.0°, 23.8° and 24.5° which should be attributed to the MFI framework topology [55]. The single peak at 24.5° further indicates the existence of orthorhombic unit cell in the 0.1 %TS-1 sample [56]. The diffraction peaks of 0.1 %TS-2 catalyst located at 7.8°、8.8°、23.1°、24.0° could be ascribed to the typical MEL framework topology [57]. Different from the TS-1 catalyst with two peaks at 23.0° and 23.8°, the TS-2 catalyst only shows single peak at 23.1° which further demonstrates the MEL framework topology [41]. Moreover, the 0.1 %Ti-β catalyst also shows the typical peaks at 2θ = 7.60、21.0° and 22.5° which are assigned to the BEA framework topology [58]. The TS-1 and TS-2 catalysts exhibit sharper peaks compared to the Ti-β catalyst. This difference may be attributed to the fact that Ti-β is typically composed of smaller particles, typically on the order of tens of nanometers.

The UV–Vis spectra showed in Fig. 3e were used to reveal the chemical state of Ti species in the framework topology. There are three different species including tetrahedral titanium (TiO_4, ~220 nm), hexagonal titanium (TiO_6, ~260 nm) and anatase TiO_2 species (~320 nm) [59–61] in the MFI, MEL and BEA framework topologies. It can be seen that the relative content of framework Ti species (TiO_4 and TiO_6 species) in 0.1 %Ti-β catalyst is higher than those in the 0.1 %TS-1 and 0.1 %TS-2 catalysts. The data reveals a discernible trend indicating a higher framework Ti content in Ti-beta compared to TS-1 and TS-2. While the results suggest that the framework Ti content in TS-1 is greater than that in TS-2, it is important to note that potential fitting errors may lead to an approximate estimation of the framework Ti content. The TEM-mapping was further used to reveal the distribution of Ti species [62] in the titanosilicalites with MFI, MEL and BEA framework topologies (Fig. 3g–i). All samples show uniform distribution of O and Si elements due to the well-crystallized framework structure which is in accordance with the XRD results. However, More blank areas without Ti distribution or aggregated Ti species (circled dotted line) reveal the non-uniform distribution of Ti species due to the formation of TiO_2 species. Compared with the Ti species in TS-1 and TS-2, the Ti-β has a more uniform distribution of Ti species. It further demonstrates that more Ti species were in incoporated into the zeolite framework which is in consistent with the UV–Vis and FT-IR spectra.

Combined with the theoretical calculations, it is found that with the decrease of LFDI (θ) from 6.67 to 3.14, the average substitution energy decreases from 0.04 to −0.50 eV, and the framework Ti species

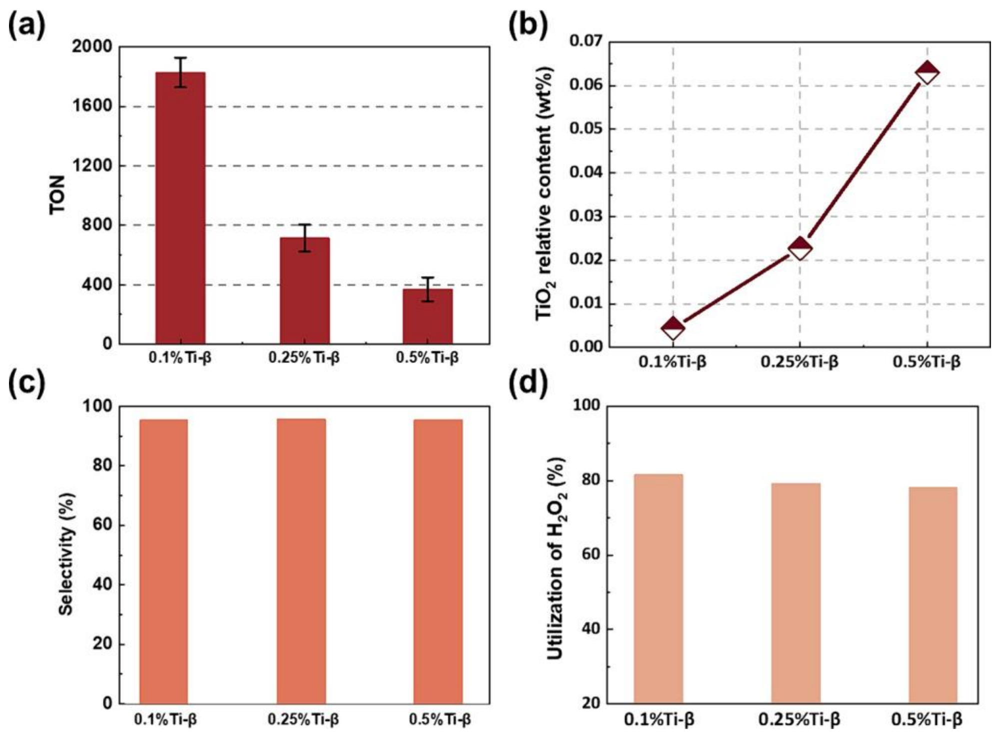

Fig. 5. The TON in 1-hexene epoxidation (a) and TiO_2 relative content (b) of Ti-β within Ti-doped range of 0.1 wt% to 0.5 wt%. The selectivity (c) and utilization of H_2O_2 (d) in 1-hexene epoxidation of Ti-β within Ti-doped range of 0.1 wt% to 0.5 wt%.

gradually increased from 67.51 % to 97.38 % (Fig. 3f and Fig. S19). Therefore, as the zeolite framework becomes distorted (indicated by a higher value of θ) due to the substitution of Ti atoms, the substitution energy gradually increases, resulting in more Ti atoms being excluded by the zeolite scaffolds and forming extra-framework TiO_2 species.

The titanosilicalites with different Ti content were further synthesized to investigate the capacity of framework Ti species in the MFI, MEL and BEA framework topologies. For the MFI framework topology (Fig. S4), the relative content of framework Ti species was gradually decreased from 74.6 % to 71.96 % when the Ti-doped content was increased from 0.1 % to 0.5 % (Fig. 4a and Fig. S5). In addition, the extra-framework TiO_2 species were increased from 25.4 % to 28.04 %. The relative content of framework Ti species in the MEL framework topology was slightly decreased from 67.51 % to 67.00 % when the Ti-doped content was increased from 0.1 % to 0.5 % (Fig. 4b and Fig. S6). The content of extra-framework TiO_2 species were about 33 %. Moreover, in the Fig. 4c and S7, the relative content of framework Ti species in the BEA framework topology (Fig. S8) was also decreased from 97.38 % to 94.54 % when the Ti-doped content was increased from 0.1 % to 0.25 %, and then it was decreased from 94.54 % to 92.44 % when the Ti-doped content was increased from 0.25 % to 0.5 %. In general, the content of framework Ti species in BEA framework was significantly higher (~90 %) than those in the MFI (~70 %) and MEL framework (~60 %) within the Ti-doped range of 0.1 wt% to 0.5 wt%. Different materials were subjected to the same atom-planting process, wherein some BEA samples exhibited a notable concentration of framework titanium species, while others displayed a limited framework titanium content. This observation substantiates the superior capacity of the BEA framework to host structural frameworks, in line with predictions from LFDI. Therefore, the BEA framework topology has higher capacity of framework Ti species than MFI and MEL framework topologies.

The reaction energy was further calculated to demonstrate the high capacity of BEA framework topology based on the following reaction [63]:

$$Zeolite[SiOH]_4 + Ti(OH)_4 = Zeolite[SiO]_4[Ti] + 4H_2O \quad (3)$$

The radar charts of reaction energy at different T sites in the MFI, MEL and BEA framework topologies were shown in Fig. 4d–f. For the MFI framework topology, the average reaction energy is about −0.405 eV (Table S1), and the standard deviation is 0.175. In the MEL framework topology, the average reaction energy is further increased to −0.380 eV (Table S1) and the standard deviation is increased to 0.230. Compared with the MFI and MEL framework topologies, the BEA framework topology has not only lower average reaction energy (-0.459 eV) but also lower standard deviation (0.088). The radar chart of BEA framework topology is smoother than those charts of MFI and MEL framework topologies due to the lower standard deviation. The lower standard deviation indicated that the reaction energies in different T sites are more concentrated [64]. Therefore, the BEA framework topologies with lower average reaction energy and standard deviation are beneficial for the incorporation of Ti atoms within the Ti-doped range of 0.1 wt% to 0.5 wt%, which is in accordance with the zeolite structure descriptor (LFDI).

3.3. *Reaction performance in 1-hexene epoxidation*

In the olefin epoxidation, the framework Ti species were identified as the real active sites in titanosilicalites, while the extra-framework TiO_2 species were found to inhibit the epoxidation reaction [65,66]. According to the prediction based on the zeolite structure descriptor (LFDI), the Ti-β catalysts with lower content of extra-framework TiO_2 species compared with TS-1 and TS-2 catalysts were synthesized. Fig. 5 and Figs. S9–S10 showed the relationship between the reaction performance and the content of framework Ti species within same framework topologies by controlling only one variable (type of titanosilicalite). The direct comparison of reaction performance of same-type titanosilicalites with different Ti contents was used to reveal the effect of different Ti species (framework Ti species and extra-framework Ti species).

With the increase of Ti content in the TS-1 catalysts from 0.1 wt% to 0.5 wt%, the TiO_2 relative content was gradually increased from 0.04 wt % to 0.23 wt%. Meanwhile, the TON of TS-1 catalysts were gradually decreased from 303 to 59 (Fig. S9). Moreover, the utilization efficiency

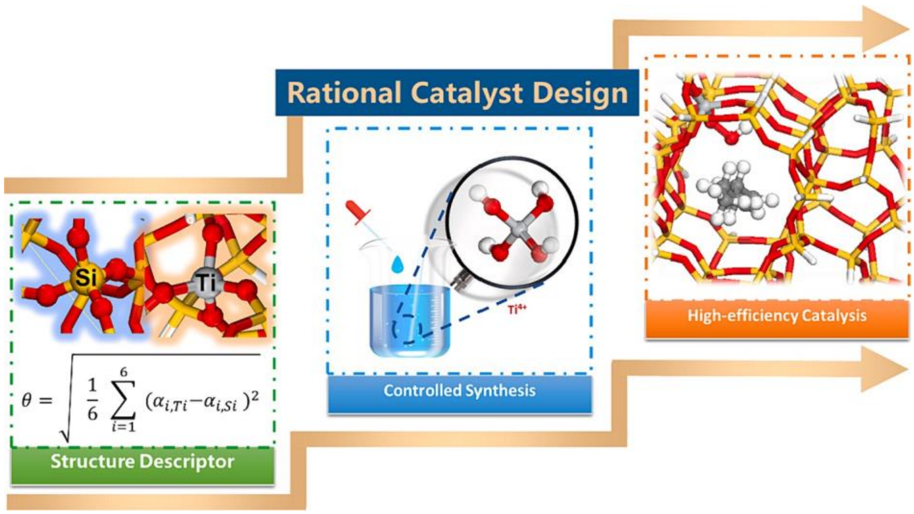

Fig. 6. The schematic diagram of ration design of metal-containing zeolites for high-efficient catalysis based on the structure descriptor.

of H_2O_2 was also gradually decreased from 63 % to 47 % due to the significantly decreased extra-framework TiO_2 species which could cause the decomposition of H_2O_2. These results showed that the framework Ti species of TS-1 are active sites for the 1-hexene epoxidation. For TS-2, the TS-2 catalysts also showed gradually decreased TON from 8 to 2 due to the gradually increasing TiO_2 relative content in the TS-2 cata- lysts from 0.06 wt% to 0.28 wt% (Fig. S10). The utilization efficiency of H_2O_2 is as low as ~ 2 % due to the extremely low TON. Therefore, the framework Ti species of TS-1 are responsible for the 1-hexene epoxidation. These results further demonstrated the importance of framework Ti species in zeolite framework for olefin epoxidation, thus confirming the meaning of zeolite structure descriptor.

The Ti-β catalysts with BEA framework topology also shows the gradually increased TON from 370 to1828 with the significantly decreased TiO_2 relative content from 0.06 wt% to 0.004 wt%. Moreover, these three titanosilicalites with BEA framework topology have similar selectivity of 1,2-epoxyhexane (~90 %). The utilization efficiency of H_2O_2 is also increased from 78 % to 82 % due to the decreased extra-framework TiO_2 species. Therefore, the design of titanosilicalites with rich framework Ti species by atom-planting method is based on the zeolite structure descriptor (LFDI) is very important for the superior reaction performance in activity and utilization of H_2O_2.

Based on the aforementioned discourse, a rational strategy for the design of metal-containing zeolites has been proposed, commencing with theoretical calculations and subsequently progressing to controlled synthesis and experimental validation (Fig. 6). The foundation of this design approach lies in the utilization of a zeolite structure descriptor, specifically the local framework disturbance index introduced in this study. The calculation of local framework disturbance index (LFDI) is based on the Ti atom in corresponding zeolite frameworks. This descriptor could serve as a basis for the rational design of not only Ti-containing zeolites but also other metal-containing zeolites (e.g., Sn). According to the data presented in Table S4, the LFDI values of Sn-zeolites exhibit the following trend: BEA < MFI < MEL. Furthermore, the relative content of framework Sn species follows the order: BEA (87.6 %) > MFI (61.1 %) > MEL (52.6 %), as depicted in Fig. S17. This alignment between the LFDI values and the distribution of framework Sn species provides additional evidence for the universality of the proposed zeolite structure descriptor.

4. Conclusion

In summary, the rational design strategy of titanosilicalites with rich framework Ti species by atom-planting method based on the zeolite structure descriptor by theoretical calculation was proposed. The local framework disturbance index (LFDI) was proposed to describe the matching degree between the metal Ti atoms and different framework topologies, thus further helping screen the better topological framework with rich low energy sites for the incorporation of Ti atom. The LFDI is positively related to the substitution energy and reaction energy during the incorporation of Ti atoms. It is found that the BEA framework with the lowest average LFDI of 3.14 and lowest average substitution energy of −0.50 eV shows the highest capacity of framework Ti species. The relative content of framework Ti species in BEA framework is 97.3 %. The Ti-β with rich framework Ti species shows outstanding 1-hexene epoxidation performances with a TON of 1827.5 and selectivity of 95.4 %. This rational design strategy can be used to guide the synthesis of highly efficient metal-containing zeolites by atom-planting method without requiring excessive experiments.

CRediT authorship contribution statement

Xuliang Deng: Investigation, Conceptualization. **Dong Lin:** Writing – review & editing, Writing – original draft, Software, Methodology, Investigation, Formal analysis, Conceptualization. **Yang Xu:** Methodology, Investigation, Conceptualization. **Xiang Feng:** Writing – review & editing, Supervision, Resources, Project administration, Methodology, Investigation, Funding acquisition, Formal analysis, Conceptualization. **De Chen:** Writing – review & editing, Supervision, Resources, Project administration. **Chaohe Yang:** Writing – review & editing, Supervision, Resources, Project administration, Funding acquisition. **Honghong Shan:** Writing – review & editing, Supervision, Resources, Investigation, Funding acquisition.

Declaration of competing interest

The authors declare that they have no known competing financial interests or personal relationships that could have appeared to influence the work reported in this paper.

Data availability

Data will be made available on request.

Acknowledgement

This work was supported by the National Natural Science Foundation of China (21978325), the Natural Science Foundation of Shandong

Province (ZR2020KB006), Fundamental Research Funds for the Central Universities (20CX06073A) and the Outstanding Youth Fund of Shandong Provincial Natural Science Foundation (ZR2020YQ17).

Appendix A. Supplementary data

Supplementary data to this article can be found online at https://doi.org/10.1016/j.cej.2024.150338.

References

[1] Q. Zhang, S. Gao, J. Yu, Metal sites in zeolites: synthesis, characterization, and catalysis, Chem. Rev. 123 (2023) 6039–6106.

[2] M. Babucci, A. Guntida, B.C. Gates, Atomically dispersed metals on well-defined supports including zeolites and metal–organic frameworks: structure, bonding, reactivity, and catalysis, Chem. Rev. 120 (2020) 11956–11985.

[3] N. Wang, Q. Sun, J. Yu, Ultrasmall metal nanoparticles confined within crystalline nanoporous materials: a fascinating class of nanocatalysts, Adv. Mater. 31 (2019) 1803966.

[4] H. Yamashita, K. Mori, Y. Kuwahara, T. Kamegawa, M. Wen, P. Verma, M. Che, Single-site and nano-confined photocatalysts designed in porous materials for environmental uses and solar fuels, Chem. Soc. Rev. 47 (2018) 8072–8096.

[5] C. Gao, F. Lyu, Y. Yin, Encapsulated metal nanoparticles for catalysis, Chem. Rev. 121 (2020) 834–881.

[6] Q. Sun, N. Wang, Q. Xu, J. Yu, Nanopore-supported metal nanocatalysts for efficient hydrogen generation from liquid-phase chemical hydrogen storage materials, Adv. Mater. 32 (2020) 2001818.

[7] N. Masoumifard, R. Guillet-Nicolas, F. Kleitz, Synthesis of engineered zeolitic materials: from classical zeolites to hierarchical core–shell materials, Adv. Mater. 30 (2018) 1704439.

[8] J. Liang, Z. Liang, R. Zou, Y. Zhao, Heterogeneous catalysis in zeolites, mesoporous silica, and metal–organic frameworks, Adv. Mater. 29 (2017) 1701139.

[9] A. Corma, Heterogeneous catalysis: understanding for designing, and designing for applications, Angew. Chem. Int. Edit. 55 (2016) 6112–6113.

[10] Q. Zhang, A. Mayoral, O. Terasaki, Q. Zhang, B. Ma, C. Zhao, G. Yang, J. Yu, Amino acid-assisted construction of single-crystalline hierarchical nanozeolites via oriented-aggregation and intraparticle ripening, J. Am. Chem. Soc. 141 (2019) 3772–3776.

[11] D. Kerstens, B. Smeyers, J. Van Waeyenberg, Q. Zhang, J. Yu, B.F. Sels, State of the art and perspectives of hierarchical zeolites: practical overview of synthesis methods and use in catalysis, Adv. Mater. 32 (2020) 2004690.

[12] X. Wang, N. Yan, M. Xie, P. Liu, P. Bai, H. Su, B. Wang, Y. Wang, L. Li, T. Cheng, The inorganic cation-tailored "trapdoor" effect of silicoaluminophosphate zeolite for highly selective CO_2 separation, Chem. Sci. 12 (2021) 8803–8810.

[13] B. Yang, Z. Zhang, C. Tian, W. Yuan, Z. Hua, S. Fan, Y. Wu, X. Tian, Selective detection of methane by HZSM-5 zeolite/Pd-SnO_2 gas sensors, Sensor. Actuat. b: Chem. 321 (2020) 128567.

[14] F. Jiao, J. Li, X. Pan, J. Xiao, H. Li, H. Ma, M. Wei, Y. Pan, Z. Zhou, M. Li, Selective conversion of syngas to light olefins, Science 351 (2016) 1065–1068.

[15] Y. Li, L. Li, J. Yu, Applications of zeolites in sustainable chemistry, Chem 3 (2017) 928–949.

[16] Y. Wang, C. Wang, L. Wang, L. Wang, F.-S. Xiao, Zeolite fixed metal nanoparticles: new perspective in catalysis, Acc. Chem. Res. 54 (2021) 2579–2590.

[17] L. Liu, A. Corma, Confining isolated atoms and clusters in crystalline porous materials for catalysis, Nat. Rev. Mater. 6 (2021) 244–263.

[18] Q. Zhang, J. Yu, A. Corma, Applications of zeolites to C1 chemistry: recent advances, challenges, and opportunities, Adv. Mater. 32 (2020) 2002927.

[19] H. Wang, L. Wang, F.-S. Xiao, METAL@ zeolite hybrid materials for catalysis, ACS Cent. Sci. 6 (2020) 1685–1697.

[20] S.M. Wu, X.Y. Yang, C. Janiak, Confinement effects in zeolite-confined noble metals, Angew. Chem. Int. Edit. 131 (2019) 12468–12482.

[21] D. Farrusseng, A. Tuel, Perspectives on zeolite-encapsulated metal nanoparticles and their applications in catalysis, New J. Chem. 40 (2016) 3933–3949.

[22] Y. Li, J. Yu, Emerging applications of zeolites in catalysis, separation and host–guest assembly, Nat. Rev. Mater. 6 (2021) 1156–1174.

[23] N. Kosinov, C. Liu, E.J. Hensen, E.A. Pidko, Engineering of transition metal catalysts confined in zeolites, Chem. Mater. 30 (2018) 3177–3198.

[24] M. Limlamthong, A.C. Yip, Recent advances in zeolite-encapsulated metal catalysts: a suitable catalyst design for catalytic biomass conversion, Bioresour. Technol. 297 (2020) 122488.

[25] Y. Chai, W. Shang, W. Li, G. Wu, W. Dai, N. Guan, L. Li, Noble metal particles confined in zeolites: synthesis, characterization, and applications, Adv. Sci. 6 (2019) 1900299.

[26] P.Y. Dapsens, C. Mondelli, J. P´erez-Ramírez, Design of Lewis-acid centres in zeolitic matrices for the conversion of renewables, Chem. Soc. Rev. 44 (2015) 7025–7043.

[27] W.G. Cui, T.L. Hu, Incorporation of active metal species in crystalline porous materials for highly efficient synergetic catalysis, Small 17 (2021) 2003971.

[28] C.P. Gordon, H. Engler, A.S. Tragl, M. Plodinec, T. Lunkenbein, A. Berkessel, J. H. Teles, A.-N. Parvulescu, C. Cop´eret, Efficient epoxidation over dinuclear sites in titanium silicalite-1, Nature 586 (2020) 708–713.

[29] R. Bai, Y. Song, L. L¨atsch, Y. Zou, Z. Feng, C. Cop´eret, A. Corma, J. Yu, Switching between classical/nonclassical crystallization pathways of TS-1 zeolite: implication on titanium distribution and catalysis, Chem. Sci. 13 (2022) 10868–10877.

[30] X. Liu, H. Song, W. Sun, B. Wang, P. Zhang, X. Yuan, Z. Wang, X. Li, Strong nano size effect of titanium silicalite (TS-1) zeolites for electrorheological fluid, Chem. Eng. J. 384 (2020) 123267.

[31] B. Chowdhury, J.J. Bravo-Sua´rez, M. Dat´e, S. Tsubota, M. Haruta, Trimethylamine as a gas-phase promoter: highly efficient epoxidation of propylene over supported gold catalysts, Angew. Chem. Int. Edit. 45 (2006) 412–415.

[32] Y. Zuo, T. Zhang, M. Liu, Y. Ji, C. Song, X. Guo, Mesoporous/microporous titanium silicalite with controllable pore diameter for cyclohexene epoxidation, Ind. Eng. Chem. Res. 57 (2018) 512–520.

[33] N.A. Grosso-Giordano, A.S. Hoffman, A. Boubnov, D.W. Small, S.R. Bare, S.I. Zones, A. Katz, Dynamic reorganization and confinement of TiIV active sites controls olefin epoxidation catalysis on two-dimensional zeotypes, J. Am. Chem. Soc. 141 (2019) 7090–7106.

[34] D. Lin, Y. Xu, X. Zheng, W. Sheng, Z. Liu, Y. Yan, Y. Cao, Y. Liu, X. Feng, D. Chen, C. Yang, Engineering Sodium-decorated Bifunctional Au-Ti Sites to Boost Molecular Transfer for Propene Epoxidation with H_2 and O_2, AlChE J., e17999.

[35] R.J. Lewis, K. Ueura, X. Liu, Y. Fukuta, T.E. Davies, D.J. Morgan, L. Chen, J. Qi, J. Singleton, J.K. Edwards, Highly efficient catalytic production of oximes from ketones using in situ–generated H_2O_2, Science 376 (2022) 615–620.

[36] C.E. Ramachandran, H. Du, Y.J. Kim, M.C. Kung, R.Q. Snurr, L.J. Broadbelt, Solvent effects in the epoxidation reaction of 1-hexene with titanium silicalite-1 catalyst, J. Catal. 253 (2008) 148–158.

[37] W. Fan, P. Wu, T. Tatsumi, Unique solvent effect of microporous crystalline titanosilicates in the oxidation of 1-hexene and cyclohexene, J. Catal. 256 (2008) 62–73.

[38] Y. Shao, J. Wang, K. Sun, G. Gao, M. Fan, C. Li, C. Ming, L. Zhang, S. Zhang, X. Hu, Cu-based nanoparticles as catalysts for selective hydrogenation of biomass-derived 5-hydroxymethylfurfural to 1, 2-hexanediol, ACS Appl. Nano Mater. 5 (2022) 5882–5894.

[39] C.-C. Tu, Y.-J. Tsou, T.D. To, C.-H. Chen, J.-F. Lee, G.W. Huber, Y.-C. Lin, Phyllosilicate-derived CuNi/SiO_2 catalysts in the selective hydrogenation of adipic acid to 1,6-hexanediol, ACS Sustainable Chem. Eng. 7 (2019) 17872–17881.

[40] R. Bai, Y. Song, R. Bai, J. Yu, Creation of hierarchical titanosilicate TS-1 zeolites, Adv. Mater. Interfaces 8 (2021) 2001095.

[41] Z. Zhang, X. Zhao, G. Wang, J. Xu, M. Lu, Y. Tang, W. Fu, X. Duan, G. Qian, D. Chen, Uncalcined TS-2 immobilized au nanoparticles as a bifunctional catalyst to boost direct propylene epoxidation with H2 and O2, AlChE J. 66 (2020) e16815.

[42] X. Liang, X. Peng, C. Xia, H. Yuan, K. Zou, K. Huang, M. Lin, B. Zhu, Y. Luo, X. Shu, Improving ti incorporation into the BEA framework by employing ethoxylated chlorotitanate as ti precursor: postsynthesis, characterization, and incorporation mechanism, Ind. Eng. Chem. Res. 60 (2021) 1219–1230.

[43] D. Lin, X. Feng, X. Zheng, Y. Xu, H. Zhao, Z. Song, L. Wang, H. Shan, F.S. Xiao, D. Chen, Y. Chaohe, Dimensional regulation of titanosilicate by kinetically controlled intergrowth crystals, Adv. Funct. Mater. 2301179 (2023).

[44] B. Wang, H. Xu, Z. Zhu, Y. Guan, P. Wu, Ultrafast synthesis of nanosized ti-Beta as an efficient oxidation catalyst via a structural reconstruction method, catal, Sci. Technol. 9 (2019) 1857–1866.

[45] Z. Zhu, H. Xu, B. Wang, J. Yin, J. Jiang, H. Lü, P. Wu, Intensified interzeolite transformation: ultrafast synthesis of active and stable ti-Beta zeolites without solvents, Chem. Commun. 55 (2019) 14279–14282.

[46] H. Lin, J. Wang, B. Gao, K. Yang, G. Lv, S. Qi, Z. Zhu, H. Lue, Solvent-free and low template content synthesis of ti-Beta zeolite via interzeolite transformation for oxidative desulfurization, Microporous Mesoporous Mater. 344 (2022) 112203.

[47] Q. Zhu, H. Liu, C. Miao, G. Wang, Y. Li, Y. Yi, Z. Feng, H. Guo, Grafting ti sites on defective silicalite-1 via $TiCl_4$ chemical vapor deposition for gas-phase epoxidation of propylene and H_2O_2 vapor, Ind. Eng. Chem. Res. 59 (2020) 2828–2838.

[48] X. Li, B. Shen, C. Xu, Interaction of titanium and iron oxide with ZSM-5 to tune the catalytic cracking of hydrocarbons, Appl. Catal. A 375 (2010) 222–229.

[49] M.A. Ardagh, D.T. Bregante, D.W. Flaherty, J.M. Notestein, Controlled deposition of silica on titania-silica to alter the active site surroundings on epoxidation catalysts, ACS Catal. 10 (2020) 13008–13018.

[50] S. Wang, P. Wang, Z. Qin, Y. Chen, M. Dong, J. Li, K. Zhang, P. Liu, J. Wang, W. Fan, Relation of catalytic performance to the aluminum siting of acidic zeolites in the conversion of methanol to olefins, viewed via a comparison between ZSM-5 and ZSM-11, ACS Catal. 8 (2018) 5485–5505.

[51] G. Yang, E.A. Pidko, E.J. Hensen, Structure, stability, and Lewis acidity of mono and double ti, zr, and sn framework substitutions in BEA zeolites: a periodic density functional theory study, J. Phys. Chem. C 117 (2013) 3976–3986.

[52] B.D. Montejo-Valencia, J.L. Salcedo-P´erez, M.C. Curet-Arana, DFT study of closed and open sites of BEA, FAU, MFI, and BEC zeolites substituted with tin and titanium, J. Phys. Chem. C 120 (2016) 2176–2186.

[53] Z. Zhu, H. Xu, J. Jiang, H. Wu, P. Wu, Hydrophobic nanosized all-silica beta zeolite: efficient synthesis and adsorption application, ACS Appl. Mater. Interfaces 9 (2017) 27273–27283.

[54] R. Millini, G. Bellussi, P. Pollesel, C. Rizzo, C. Perego, Beyond TS-1: background and recent advances in the synthesis of ti-containing zeolites, Microporous Mesoporous Mater. 346 (2022) 112286.

[55] X. Feng, N. Sheng, Y. Liu, X. Chen, D. Chen, C. Yang, X. Zhou, Simultaneously enhanced stability and selectivity for propene epoxidation with H_2 and O_2 on au catalysts supported on nano-crystalline mesoporous TS-1, ACS Catal. 7 (2017) 2668–2675.

[56] X. Feng, X. Duan, G. Qian, X. Zhou, D. Chen, W. Yuan, Au nanoparticles deposited on the external surfaces of TS-1: enhanced stability and activity for direct

propylene epoxidation with H_2 and O_2, Appl. Catal. b: Environ. 150 (2014) 396–401.
[57] J.S. Reddy, R. Kumar, Synthesis, characterization, and catalytic properties of a titanium silicate, TS-2, with MEL structure, J. Catal. 130 (1991) 440–446.
[58] Z. Yang, Q. Yu, Y. Guo, X. Wu, H. Wang, J. Han, Q. Ge, X. Zhu, Effect of postsynthesis preparation methods on catalytic performance of ti-Beta zeolite in ketonization of propionic acid, Microporous Mesoporous Mater. 330 (2022) 111625.
[59] Q. Guo, K. Sun, Z. Feng, G. Li, M. Guo, F. Fan, C. Li, A thorough investigation of the active titanium species in TS-1 zeolite by in situ UV resonance raman spectroscopy, Chem.- Eur. J. 18 (2012) 13854–13860.
[60] W. Xu, T. Zhang, R. Bai, P. Zhang, J. Yu, A one-step rapid synthesis of TS-1 zeolites with highly catalytically active mononuclear TiO_6 species, J. Mater. Chem. A 8 (2020) 9677–9683.
[61] Y. Wang, L. Li, R. Bai, S. Gao, Z. Feng, Q. Zhang, J. Yu, Amino acid-assisted synthesis of TS-1 zeolites containing highly catalytically active TiO_6 species, Chin. J. Catal. 42 (2021) 2189–2196.
[62] D. Lin, Q. Zhang, Z. Qin, Q. Li, X. Feng, Z. Song, Z. Cai, Y. Liu, X. Chen, D. Chen, S. Mintova, C. Yang, Reversing titanium oligomer formation towards high-efficiency and green synthesis of titanium-containing molecular sieves, Angew. Chem. Int. Edit. 60 (2021) 3443–3448.
[63] B.D. Montejo-Valencia, M.C. Curet-Arana, DFT study of the Lewis acidities and relative hydrothermal stabilities of BEC and BEA zeolites substituted with ti, sn, and ge, J. Phys. Chem. C 119 (2015) 4148–4157.
[64] Z. Luo, J.H. Koo, Quantifying the dispersion of mixture microstructures, J. Microsc. 225 (2007) 118–125.
[65] D. Lin, X. Zheng, X. Feng, N. Sheng, Z. Song, Y. Liu, X. Chen, Z. Cai, D. Chen, C. Yang, Enhancing the dynamic electron transfer of au species on wormhole-like TS-1 for boosting propene epoxidation performance with H_2 and O_2, green, Energy Environ. 5 (2020) 433–443.
[66] N. Sheng, Z. Liu, Z. Song, D. Lin, X. Feng, Y. Liu, X. Chen, D. Chen, X. Zhou, C. Yang, Enhanced stability for propene epoxidation with H_2 and O_2 over wormhole-like hierarchical TS-1 supported au nanocatalyst, Chem. Eng. J. 377 (2019) 119954.